DOI: 10.26599/FSHW.2025.9250839

Contents lists available at SciOpen

Food Science and Human Wellness

journal homepage: https://www.sciopen.com/journal/2097-0765

China Food Publishing Co.

Compartmentalized multi-enzyme immobilization in hierarchical shell-shell structure for glucose detection

Lixue Zhao[1], Minsong Zhang[1], Shumao Yang[1], Tongyue Zhu[1], ZichenWang[1], Yali Bi[1,*], Hongwu Wang[2,*], Jiandong Cui[1,2,*]

[1]*State Key Laboratory of Food Nutrition and Safety, Laboratory of Industrial Fermentation Microbiology, Ministry of Education; Tianjin University of Science and Technology, No 29, 13th, Avenue, Tianjin Economic and Technological Development Area (TEDA), Tianjin 300457, China.*

[2]*Guangdong Engineering Technology Research Center of Food & Agricultural Product Safety Analysis and Testing, School of Food & Pharmaceutical Engineering, Zhaoqing University, Zhaoqing 526061, People's Republic of China*

ABSTRACT: Recent years, incorporation of multiple enzymes into matrix is considered as promising candidates for constructing highly sensitive glucose-responsive systems. However, the stochastic nature of traditional multi-enzyme immobilization techniques makes it challenging to precisely control the spatial arrangement of enzyme molecules. Here, a new hierarchical shell-shell (HSS) multi-enzyme structure was constructed using interfacial growth method and colloidal hydrated zinc sulphate to be used as a soft template (Cyt C@HSS@GOx). In this process, glutathione (GSH) hybrid ZIF-67 was used as the guest MOF and hollow ZIF-8 as the host MOF. The resultant Cyt C@HSS@GOx exhibited high activity by separating cytochrome C (Cyt C) and glucose oxidase (GOx) in two independent compartments. This method can accurately locate the spatial position of multiple enzymes, weaken enzyme-to-enzyme inhibition, and enhance the channeling effect of substrates, thus improving the catalytic performance of multiple enzymes. The resulting Cyt C@HSS@GOx showed 230% higher activity than free enzymes, and maintained good stability under extreme pH and temperature conditions. Furthermore, Cyt C@HSS@GOx demonstrated 71.25% retention of its initial activity following seven cycles, providing good reusability. Particularly, Cyt C@HSS@GOx has been demonstrated to possess a glucose detection limit as low as 0.38 μmol/L, with a reaction time of only three minutes. This strategy provides a rapid and accurate glucose detection method.

Keywords: Compartmentalized enzyme immobilization; MOFs; Shell-Shell structure; Glucose detection

1. Introduction

Glucose is a monosaccharide that is distributed extensively throughout nature and is one of the nutrients necessary for the body's energy metabolism and life support [1]. Nevertheless, abnormal glucose levels within the body have been demonstrated to be a contributing factor to the development of a range of diseases, including but not limited to cardiovascular lesions, myocardial infarction, sudden cerebral death and diabetes. Among these diseases, diabetes has become a public problem that seriously threatens the lives and health of human beings [2]. Generally, many foods contain glucose such as fruits, beverages, bread, and dairy products.

***Corresponding author**
jdcui@tust.edu.cn

Received 21 March 2025
Received in revised from 11 May 2025
Accepted 28 July 2025

For patients with diabetes or those who need to control blood sugar, the intake of these high glucose foods should be minimized. Consequently, glucose testing is imperative to ensure the safety and nutritional value of food products [3].

In past few years, a variety of glucose detection methods have been established, including electrochemical methods [4, 5], fluorescence methods [6] and photothermal methods [7]. However, these methods need a series of complex pre-processing procedures, time-consuming detection processes, and the utilization of costly instruments. In comparison with alternative analytical techniques employed for detection, enzymatic assays offer distinct advantages in terms of simplicity, practicality and high sensitivity. The majority of enzymatic assays for glucose concentration rely on the catalysis of glucose oxidase, forming gluconic acid and hydrogen peroxide from glucose and oxygen. The amount of hydrogen peroxide produced can be derived from the catalysis of the color development reaction of hydrogen peroxide oxidation of various substrates by peroxidase. Consequently, the presence of hydrogen peroxide and glucose can be detected through the utilization of enzymatic methods. However, the inherent instability of free enzymes, such as high sensitivity to extreme temperature and pH, as well as low tolerance to most organic solvents, which will limit the specific application of the enzyme system in practice [8, 9]. Enzyme immobilization technology, in which the enzyme molecule is immobilized on a carrier material while maintaining its spatial structural integrity, is an effective method to improve the free enzyme that cannot be recovered and has poor stability.

The majority of traditional multi-enzyme co-immobilized materials have been observed to immobilize multi-enzyme on a single carrier in a disordered manner. However, the use of traditional co-immobilization methods in the evolution of multi-enzyme systems has been shown to present a number of significant challenges such as the absence of an effective modulation mode for the cascade reaction, the random positioning of enzymes and the potential for interference with the cascade reaction due to mutual contact between enzymes. It is therefore evident that the effective structuring of multi-enzyme biocatalysts and optimization of spatial assembly are essential to promote the synergistic effect of multi-enzyme; in order to meet the increasingly complex demands of biocatalysts and chemical synthesis [10]. The compartmentalization strategy involves the segregation of each enzyme into a discrete compartment, which can be isolated to avoid the potential disruption to enzyme activity from the harsh external environment and the phenomenon of mutual inhibition between enzyme molecules [11, 12]. For instance, Zhang [13] developed and constructed a hierarchical yolk-shell@-shell nanoreactor, using mesoporous yolk-shell nanostructures to achieve the spatial localization of metal nanoparticles and enzymes, thereby facilitating mass transfer between the yolk and shell. The spatial separation of the Pd nanoparticles and CALB was achieved through the placement of the nanoparticles at different locations. Separate immobilization of Pd and CALB resulted in higher catalytic efficiency compared to mixed catalysts. Liu [14] constructed a colloidal multi-enzyme system for the first time using a Pickering emulsion with a SiO_2-stabilized W/O template, in which hydrophilic GOx was encapsulated in the inner cavity of an aqueous environment, and hydrophobic CALB was immobilized on the SiO_2 shell by adsorption. Obviously, compartmentalization represents a more accessible and effective

enhancement strategy than the construction of complex and uncontrollable substrate channels, especially in the context of spatially distributed multi-enzyme compartmentalization [15].

The purpose of this work was to develop a compartmentalized multi-enzyme immobilization in hierarchical shell-shell structure for glucose detection. The approach entailed the immobilization of cytochrome C (Cyt C) and glucose oxidase (GOx) as model enzymes within a layered shell-shell metal-organic framework (MOF) carrier. We employed an interfacial growth method by using GSH hybrid zeolitic imidazolate framework-67 (GZIF-67) as the guest MOF and the host MOF for the study is hollow zeolitic imidazolate framework-8 (HZIF-8). Cyt C encapsulated in HZIF-8 (Cyt C@HZIF-8) and GOx encapsulated in GZIF-67 (GZIF-67@GOx), GOx@GZIF-67 grows on the surface of Cyt C@HZIF-8 to form Cyt C@HZIF-8@GZIF-67@GOx (Cyt C@HG@GOx). Subsequently, the GZIF-67 template was removed after the addition of shells to the surface of Cyt C@HG@GOx, resulting in the formation of a hierarchical shell-shell multi-enzyme structure (Cyt C@HSS@GOx). Moreover, the Cyt C@HSS@GOx structure demonstrated the capacity to facilitate dual enzyme cascade reaction in one procedure. As a result, the Cyt C@HSS@GOx exhibited superior performance for glucose detection. The detection limit was 0.38 μmol/L, with a reaction time of only three minutes. The present method has superior detection practicability in comparison to non- compartmentalized dual enzyme immobilization (Cyt CGOx@HZIF-8).

2. Experiments

2.1 Materials

Zinc sulfate heptahydrate (99%, $ZnSO_4 \cdot 7H_2O$), 2-Methylimidazole (98%, 2-Melm), Cobalt nitrate hexahydrate (99%, $Co(NO_3)_2 \cdot 6H_2O$), 2,2′-azino-bis (3-ethylbenzothiazoline-6-sulfonic acid) (98%, ABTS), Glutathione (GSH), Polyvinylpyrrolidone (PVP), 3-Aminopropyltriethoxysilane (APTES), Pluronic F-127, Tetraethoxysilane (TEOS) were purchased from Aladdin (Shanghai, China). Cytochrome C (95%, BR, horse heart, Cyt C), Glucose oxidase (BR, 50 ku, GOx), Fluorescein isothiocynate (95%, FITC) and Rhodamine B (70%, RhB) were obtained from yuanye bio-technology (Shanghai, China). D-Glucose (99.8%), Gradehydrogen peroxide (30%, H_2O_2), Dimethyl sulfoxide (DMSO), Methanol anhydrous were purchased from solarbio science & technology (Beijing, China). All the other chemicals were of analytical.

2.2 The preparation of Cyt C@HZIF-8 and Cyt CGOx@HZIF-8

HZIF-8 was synthesized by the method of Feng et al [16]. For Cyt C@HZIF-8, The experimental conditions were comparable to those of HZIF-8, with the exception of the additional Cyt C (0.6 mg/mL). For Cyt CGOx@HZIF-8, the experimental conditions were comparable to those of HZIF-8, with the exception of the additional Cyt C (0.6 mg/mL) and GOx (0.8 mg/mL).

2.3 The preparation of Cyt C@HG@GOx

GZIF-67 was synthesized by the method of Shen et al [17]. Add the above Cyt C@HZIF-8 to 2 ml of GOx solution, followed by GSH and PVP, and finally the addition of 2 mL of $Co(NO_3)_2 \cdot 6H_2O$ solution and 2 mL of 2-Melm solution, the next step is to allow the mixture to stand at room temperature for 4 h. This is then

followed by the process of centrifugation and washing with water, in order to obtain the desired product Cyt C@HG@GOx.

2.4. The preparation of Cyt C@HSS@GOx

Add 2 mL of water to the prepared Cyt C@HG@GOx, followed by 10 μL of APTES and stir for 1 h at room temperature. After centrifugation, 2 mL of water was added to the centrifugation product, then Pluronic F-127 and TEOS were added and stirred for 30 minutes. The product was finally centrifuged and washed with water. Subsequently, the GZIF-67 template was allowed to place for 30 minutes in phosphate buffer and washed with water to obtain the final shell-shell mulyi-enzyme structure Cyt C@HSS@GOx.

2.5 Enzymatic activity assay

For Cyt C, the reaction system consisted of 700 μL (10 mmol/L, pH 8.0) Tris-HCl, 100 μL (10 mmol/L) H_2O_2, 100 μL (5.64 mmol/L) ABTS, and 100 μL (0.6 mg/mL protein) Cyt C or immobilized Cyt C. The concentration of oxidized ABTS was calculated by measuring the increase in absorbance of the reaction at 415 nm for two minutes. Cyt C activity was defined as the amount of enzyme required to oxidize 1 μmol/L ABTS per minute as 1 U. For the glucose detection, the cascade reaction of GOx and Cyt C is initiated by the oxidation of glucose by GOx, resulting in the generation of hydrogen peroxide. Subsequently, the oxidation of ABTS to the chromophore $ABTS^+$ is catalyzed by Cyt C, leading to the observed change in color. Standard curves are plotted using different concentrations of glucose standards in this assay system. The glucose content is then determined by calculating the extinction coefficient value and entering it into the standard curve. The reaction system consisted of 800 μL (10 mmol/L, pH 8.0) of GO/Tris-HCl, 100 mL (5.64 mmol/L) of ABTS, and 100 mL of immobilized Cyt C/ GOx. The reaction was carried out using the same method as for the Cyt C. The detection limit was calculated by carrying out for 3 minutes at room temperature.

detection limit (LOD)=$3\sigma/S$ (1)

where S is the linear slope and σ is the standard deviation of 11 blank sample test values.

To verify the practicability of the biosensor, we randomly detected glucose concentration in three kinds of common foods: glucose cube, glucose oral solution and Cola.

2.6 Measurement of kinetic parameters

Kinetic parameters were determined by examining the initial reaction rate at different glucose concentrations. Enzyme activity was determined at glucose concentrations of 5-300 μmol/L. All kinetic parameters were calculated using the Michaelis-Menten equation. The kinetic parameters of Cyt C, GOx and immobilized Cyt C and GOx were determined using Equation 2；

$$V_0 = \frac{V_{max}[S]}{(K_m + [S])} \quad (2)$$

where V_{max} is the maximum reaction rate and V_0 is the initial catalytic rate. K_m is the MichealisMenten constant and [S] is the initial substrate concentration.

2.7 Synthesis of RhB or FITC labeled proteins

For RhB-Cyt C or FITC-GOx, 1.3 mg RhB or FITC was dissolved in 0.5 mL dimethyl sulfoxide and 2 mg Cyt C or 1.5 mg GOx was dissolved in 2.5 mL carbonate buffer (10 mmol/L, pH 9.8). The mixture was stirred for 3 hours and dialyzed with carbonate buffer (10 mmol/L, pH 9.8) for 2 days until residual RhB or FITC was removed, and finally the labelled enzyme solution was immobilized and visualized by CLSM.

2.8 Characterization of Cyt C@HZIF-8, Cyt C@HG@GOx and Cyt C@HSS@GOx

Scanning electron microscopy (SEM) was performed on a FEI-Apreo manufactured in the Czech Republic, USA, at 2 kV. Transmission electron microscopy (TEM) images and energy dispersive spectrum (EDS) analyses were performed on a Talos G2 200X at 200 kV. Laser scanning confocal microscopy (CLSM) was used to detect fluorescence using an Olympus FV1000 model. FTIR spectra were recorded using a NICO-LET IS50 instrument against a KBr background. N2 adsorption-desorption analyses were performed at 300 ℃ using a Brunauer-Emmett-Taylor (BET, AUTOSORB IQ).

3. Results and discussion

3. 1 Synthesis and characterization of immobilized enzymes

The uncomplicated self-assembly procedure of the immobilized multi enzyme is depicted in Fig. 1. Firstly, Cyt C was immobilized within the interior of HZIF-8 by the embedding method to form Cyt C@HZIF-8. SEM images showed that Cyt C@HZIF-8 exhibited a 0.5 μm spherical morphology (Fig. 2a). TEM images demonstrated that it possessed a core-shell structure (Fig. 2b). The results indicated that the $ZnSO_4 \cdot 7H_2O$ colloid has undergone dissolution when the Cyt C@HZIF-8 was converted to the aqueous phase, resulting in a hollow-type structure. Subsequently, Cyt C@HG@GOx was synthesized by employing the interfacial growth method to facilitate the growth of GZIF-67 on the surface of HZIF-8, with GOx embedded in GZIF-67 [18, 19]. SEM images revealed the formation of an additional layer of spheres on the outer layer of the Cyt C@HZIF-8, identified as GZIF-67 (Fig. 2c and d). Subsequently, a hierarchical of silica shell was deposited on the outer layer of Cyt C@HG@GOx, and the template GZIF-67 was removed, resulting in the formation of a hierarchical shell-shell multi-enzyme structure (Cyt C@HSS@GOx) (Fig. 2e and f) [20].

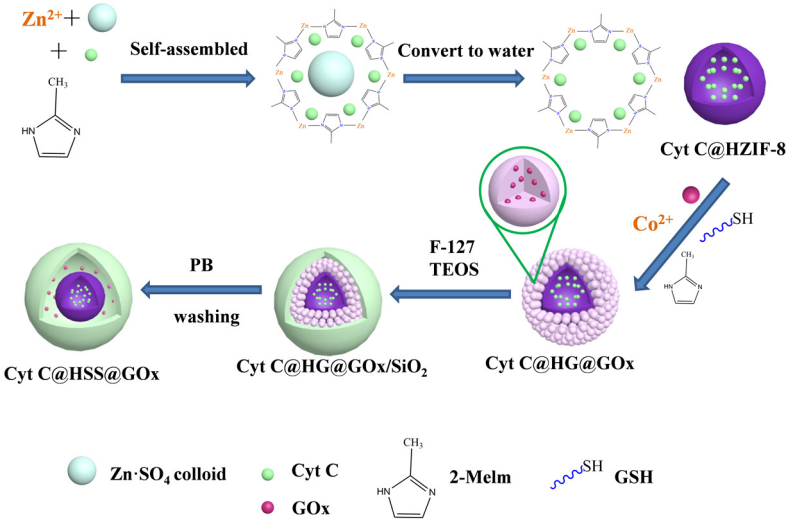

Fig. 1 Schematic for synthesis process of Cyt C@HSS@GOx.

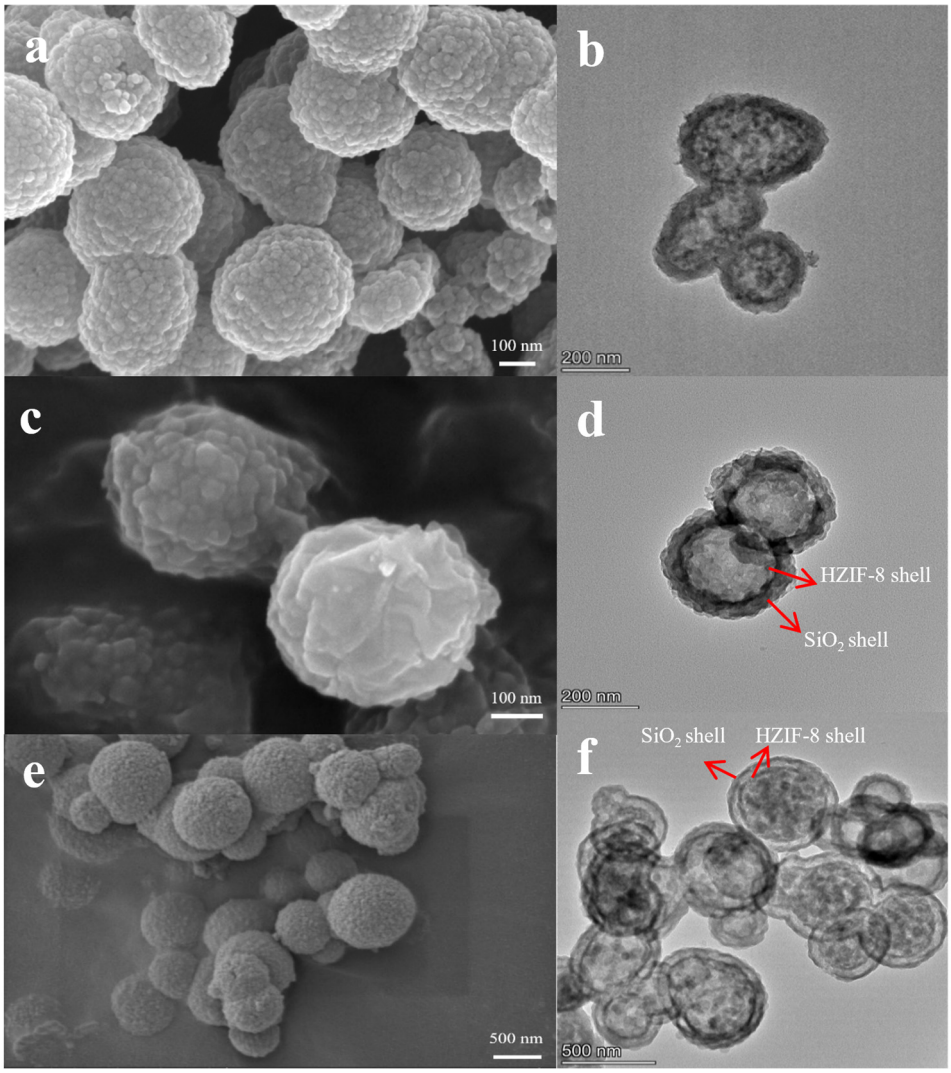

Fig. 2 SEM and TEM images of (a, b) Cyt C@HZIF-8; (c, d) Cyt C@HG@GOx; (e, f) Cyt C@HSS@GOx.

To verify the successful immobilization of Cyt C and GOx on Cyt C@HSS@GOx, EDS analysis was employed, the results of which are presented in Fig. 3. The existence of C, N, Zn and S elements in Cyt C@HZIF-8 provides evidence that ZIF-8 has been formed. Furthermore, Cyt C is an iron-containing enzyme, with an iron atom situated within its active site [21]. The existence of the Fe element was clearly observed in Cyt C@HZIF-8, which proves the existence of the Cyt C molecule in HZIF-8. The presence of the Co element in Cyt C@HG@GOx provides evidence that GZIF-67 has grown on the surface of HZIF-8 (Fig. 3a). The disappear of the Co element in Cyt C@HSS@GOx and the presence of the Si element provided evidence that silica shells have formed and that the template GZIF-67 has been successfully removed (Fig. 3b). The CLSM results are presented in Fig. S1. Cyt C@HSS@GOx, which contains Cyt C, exhibited fluorescence (RhB labelling) (Fig. 4a), while Cyt C@HSS@GOx, which contains GOx, displays green fluorescence (FITC labelling) (Fig. 4b). The Cyt C@HSS@GOx complex exhibits fluorescence in two superimposed colors (Fig. 4c). These findings suggest that RhB-Cyt C and FITC-GOx co-exist in Cyt C@HSS@GOx, thereby indicating the formation of a multi-enzyme system.

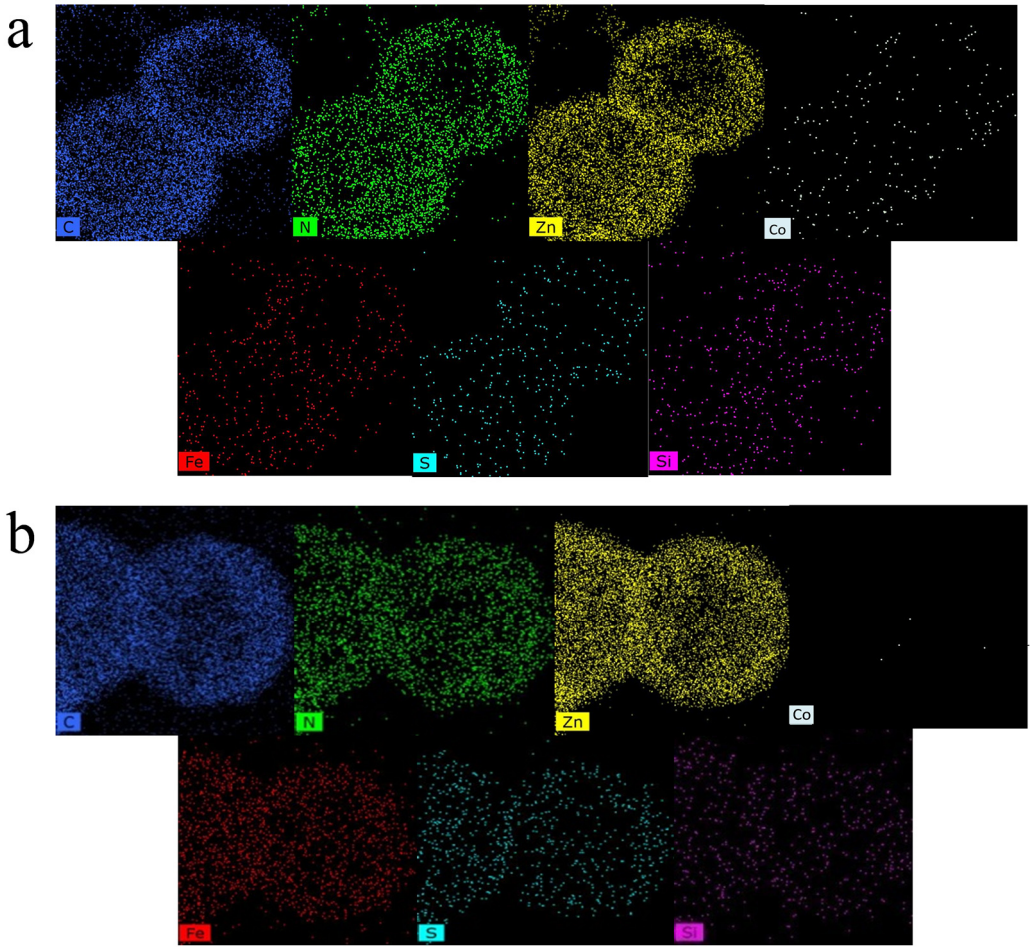

Fig. 3 (a) EDS mapping of elemental distributions of Cyt C@HG@GOx; (b) EDS mapping of elemental distributions of Cyt C@HSS@GOx.

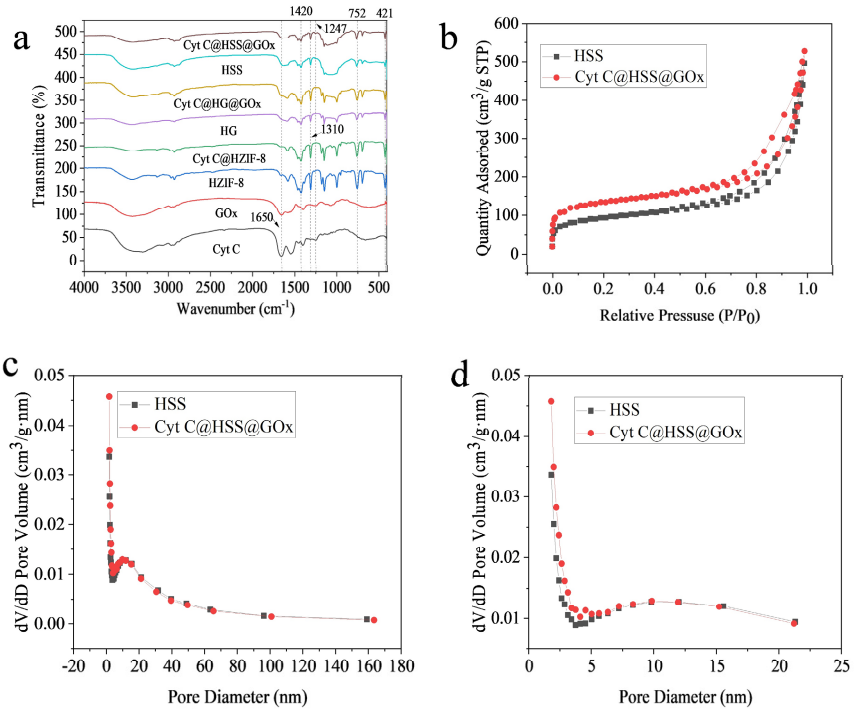

Fig. 4 (a) FTIR spectra of Cyt C, GOx, HZIF-8, Cyt C@HZIF-8, HG, Cyt C@HG@GOx, HSS and Cyt C@HSS@GOx.; (b) N_2 adsorption–desorption isotherm of HSS and Cyt C@HSS@GOx; (c, d) Micropores and mesopores distribution of HSS and Cyt C@HSS@GOx calculated by the methods of DFT.

The peak at 1650 cm-1 observed in Cyt C and GOx samples belongs to the amide I band. However, the characteristic peak at 1650 cm-1 was not observed in Cyt C@HZIF-8, Cyt C@HG@GOx and Cyt C@HSS@GOx. (Fig. 4a), suggesting that Cyt C and GOx were not present on the surface of the HSS but encapsulated within the carrier [22]. The peaks at 421, 752, 1310 and 1420 cm^{-1} are due to Zn-N and Co-N stretching as well as imidazole ring stretching vibrations, suggesting the successful formation of ZIF-8 and ZIF-67 [23]. The peak at 1247 cm^{-1} for the Si-O functional group provides evidence that the formation of silica shells has been successfully achieved. The N_2 adsorption/desorption isotherms demonstrate that both HSS and Cyt C@HSS@GOx exhibit type IV isotherms at high relative pressures with notable hysteresis loops, indicative of the existence of mesopores (Fig. 4b). Following the calculation of the pore size via the DFT method (Fig. 4c and d), it was observed that the primary distribution of the HSS and Cyt C@HSS@GOx nanochannels was situated at 10 nm. Following the immobilization of the enzyme, an increase in surface area and volume was observed. Since HSS is a porous material, the pore structure of the carrier provided additional surface area and space for the enzyme. This leads to an increase in overall specific surface area and pore volume [24]. The average pore size analysis showed that the average pore size of HSS is 9.05 nm, which was slightly greater than that of Cyt C@HSS@GOx, since the enzyme molecules are embedded in the carrier, and the porous material itself has a wide pore size distribution, during immobilization, it is the smaller pore sizes that are occupied by enzyme molecules, whereas the larger pore sizes are relatively less likely to be affected. This is because the specific surface area and pore volume increase due to the porous nature of the carrier. However, it has been demonstrated that the interaction between the enzyme molecules and the porous structure results in a narrowing of the pore channels and a decrease in the average pore size [25] (Table S1). Consequently, the existence of mesopores of Cyt C@HSS@GOx is able to establish superior contact with the substrate during the catalytic reaction.

3.2 Catalytic performance of Cyt C@HSS@GOx

Firstly, effects of enzyme concentration on the multi-enzyme immobilization preparation were optimized, and it was found that the enzyme activity reached its maximum value, approximately 230%, with Cyt C additions of 0.6 mg/mL and GOx of 0.4 mg/mL (Fig. 5a and 5b). To demonstrate the advantages of the Cyt C@HSS@GOx segregated immobilization approach, a comparison study of the enzyme activities of the was conducted between the free enzymes and the various stages of the synthesis process (Fig. 5c). The removal of the templates resulted in a notable enhancement in enzyme activity, as evidenced by a 2.3-fold increase in Cyt C@HSS@GOx and a 1.3-fold increase in Cyt C@HG@GOx compared to the free enzymes. Meanwhile, the immobilization efficiency of Cyt C@HG@GOx was found to be 90.5%, which was slightly lower than that of Cyt C@HSS@GOx (92.1%) (Table 1). A reduction in the immobilization efficiency may be attributable to the leakage of enzyme during template removal. Nevertheless, the expression activity of Cyt C@HSS@GOx remained about 1.3 times higher than Cyt C@HG@GOx. This suggests that the removal of the template resulted in an increase in enzyme activity, which caused the enzyme to become free within the cavity and in closer contact with the substrate, and reduces mass transfer resistance [26]. The higher enzyme

activity was found in Cyt C@HG@GOx and Cyt C@HSS@GOx may be due to the fact that fixation of Cyt C@HZIF-8 induces a conformational change in Cyt C [27, 28]. The active center of Cyt C contains a heme iron (Fe) ion, typically in the form of Fe(III). In certain conditions, Fe(III) can undergo reduction to Fe(II), thus facilitating electron transfer between the enzyme and the substrate. This results in a substantial alteration to the catalytic activity of the enzyme[29]. As a result, the enzyme activity after the cascade of Cyt C and GOx is also higher than that of the free enzyme. Furthermore, a comparison was conducted between the compartmentalized immobilized enzyme of this study and the conventional randomly immobilized dual enzyme (Fig. 5d), including the immobilization of Cyt C and GOx as a catalytic system in HZIF-8, as well as the immobilization of HZIF-8 and GZIF-67. It was determined that the Cyt C@HSS@GOx exhibited higher activity than several other conventional randomly immobilized dual enzyme. This is due to the fact that it allows the enzyme and enzyme molecules to reduce their mutual inhibition through the use of a segregation approach [30].

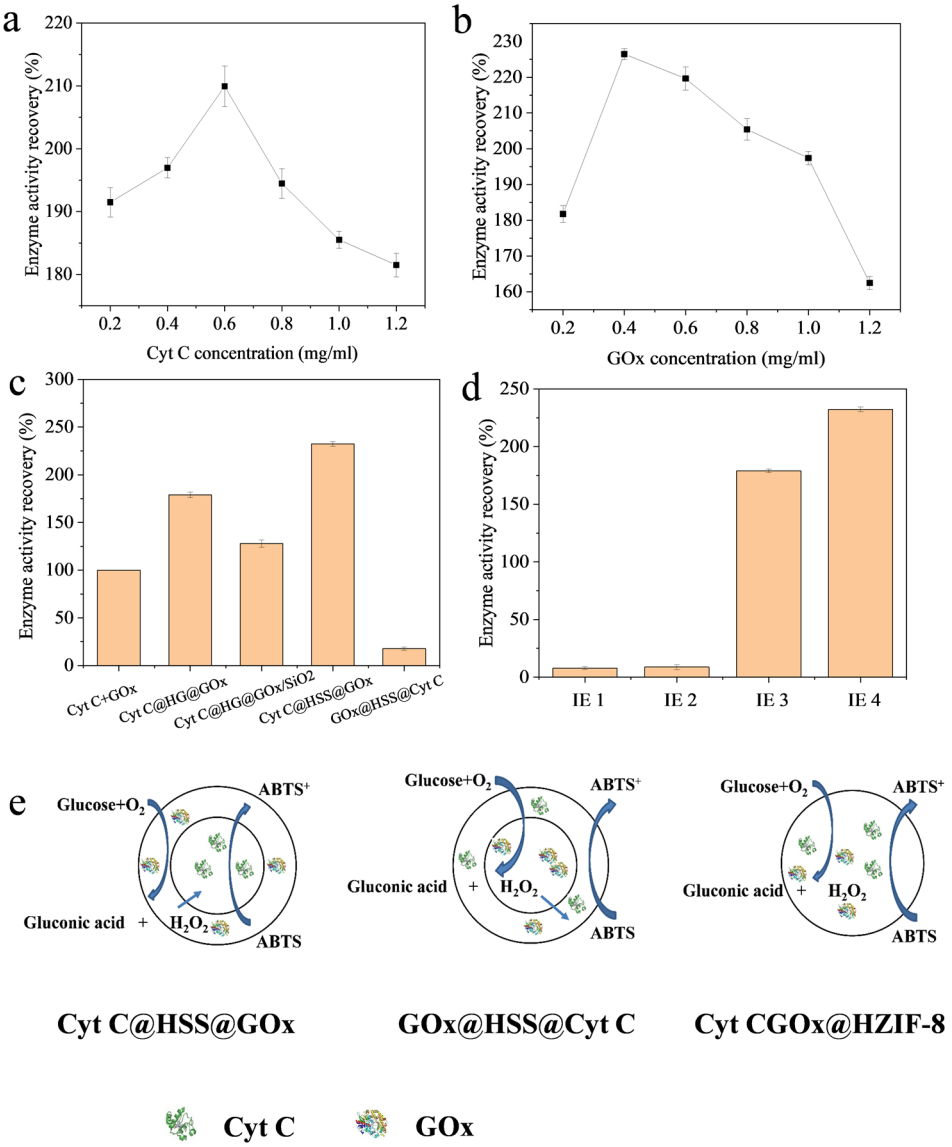

Fig. 5 Cyt C@HSS@GOx (a) Cyt C; (b) Effects of GOx concentrations on enzyme activity; (c) Comparison of the immobilization process and the recovery of enzyme activity in the exchange enzyme immobilization sequence; (d) Comparison of enzyme activity recovery between different immobilized enzymes. Where IE 1 is Cyt C/GOx@HZIF-8; IE 2 is Cyt C@HZIF-8+GOx@HZIF-8; IE 3 is Cyt C@HZIF-8+GOx@GZIF-67; IE 4 is Cyt C@HSS@GOx; (e) Substrate channel schematic of the three immobilization sequences.

Table 1 Immobilization efficiency and activity recovery of Cyt C@HG@GOx and Cyt C@HSS@GOx

Sample	Immobilization efficiency(%)	Enzyme activity recovery(%)
Cyt C@HG@GOx	90.5%	178.94%
Cyt C@HSS@GOx	92.1%	232.35%

Furthermore, by fitting the non-linear curve of immobilized enzyme versus glucose concentration, the following kinetic parameters can be obtained. Although both Cyt C@HG@GOx and Cyt C@HSS@GOx have higher Km values than free Cyt C, Cyt C@HSS@GOx has a Km value 1.16 times lower than Cyt C@HG@GOx (Table 2). This suggests that Cyt C@HSS@GOx has a considerably stronger affinity for the substrate than Cyt C@HG@GOx. The increased in the affinity of Cyt C@HSS@GOx for the substrate can be attributed to its hollow shell-layer structure, which not only improves the mass transfer, but also improves the contact between the enzyme and the substrate [31]. It was observed that the Vmax and Kcat values of Cyt C@HG@GOx and Cyt C@HSS@GOx were higher than those of free Cyt C. The increase in Vmax and Kcat can be attributed to the interaction between Cyt C and imidazole in the ZIF-8, which improves the catalytic activity of Cyt C [32].

Table 2 Kinetic parameters for free enzymes, Cyt C@HG@GOx and Cyt C@HSS@GOx

Sample	K_m (mmol/L)	V_{max} (r/min)	Kcat (min^{-1})
Free enzymes	6.95	0.0115	0.0071
Cyt C@HG@GOx	9.75	0.0191	0.0118
Cyt C@HSS@GOx	8.34	0.0295	0.0182

3.3 Substrate channeling effect

In general, the substrate channel has a decisive influence on the efficacy of the cascade catalytic system and can affect the efficiency of the final cascade reaction. To more clearly illustrate the superior substrate channeling effect of Cyt C@HSS@GOx, we conducted a comparative analysis of the absorbance values of free enzyme, Cyt C@HG@GOx and Cyt C@HSS@GOx at varying substrate concentrations and different reaction times (Fig. 6a and 6b). The findings revealed that the absorbance value of Cyt C@HSS@GOx was consistently higher than that of Cyt C@HG@GOx and free enzyme, and the trend of increasing light absorption values is higher. Consequently, the reaction rate was found to be considerably faster for Cyt C@HSS@GOx [33]. Transient time τ is the time at which the intermediate product H_2O_2 reaches steady state, which is the phase in an enzyme cascade system before the steady state rate is reached. Therefore, τ(s) can be obtained from the fitted linear relationship between the amount of final product and the reaction time at τ intersecting the abscissa time as the H_2O_2 yield plateaus. Rapid delivery of H_2O_2 shortens the time to reach steady state, resulting in a smaller τ [34, 35]. Cyt C@HSS@GOx also has a low τ (Fig. 6b). The results indicated that the co-immobilized system allows for the free movement of Cyt C and GOx within the cavity, facilitating a more rapid transfer of H_2O_2 molecules produced by GOx to the active site of Cyt C. This enhanced substrate channeling is attributed to the improved contact between the active sites of Cyt C and GOx [36]. In contrast, following the exchange of the immobilization order of the two enzymes, a significant decrease in enzyme activity was noticed (Fig. 5c). In the presence of immobilized GOx in the outer shell and immobilized Cyt C in the inner shell, the initial reaction of GOx with glucose results in producing gluconic

acid and H_2O_2, at this stage, the intermediate product is located in the outer shell, it then continues to diffuse inwards to the inner shell, where it reacts with Cyt C to color ABTS (Fig. 5e). At this point, the reaction pathway is from the outside to the inside. GOx is localized in the outer layer, which facilitates its proximity to the substrate and enhances its catalytic efficiency [37]; When Cyt C is immobilized in the outer shell and GOx is immobilized in the inner shell, the external glucose first reacts with the internal GOx to produce H_2O_2. The internal H_2O_2 then diffuses outward to react with Cyt C, which lengthens the reaction pathway and reduces the speed of color development, resulting in a lower absorption value at the same time; The mixing and immobilization of Cyt C and GOx results in the prolonged accumulation of the intermediate product H_2O_2. This, in turn, inhibits the initial step of the reaction, thereby decreasing the reaction rate [38].

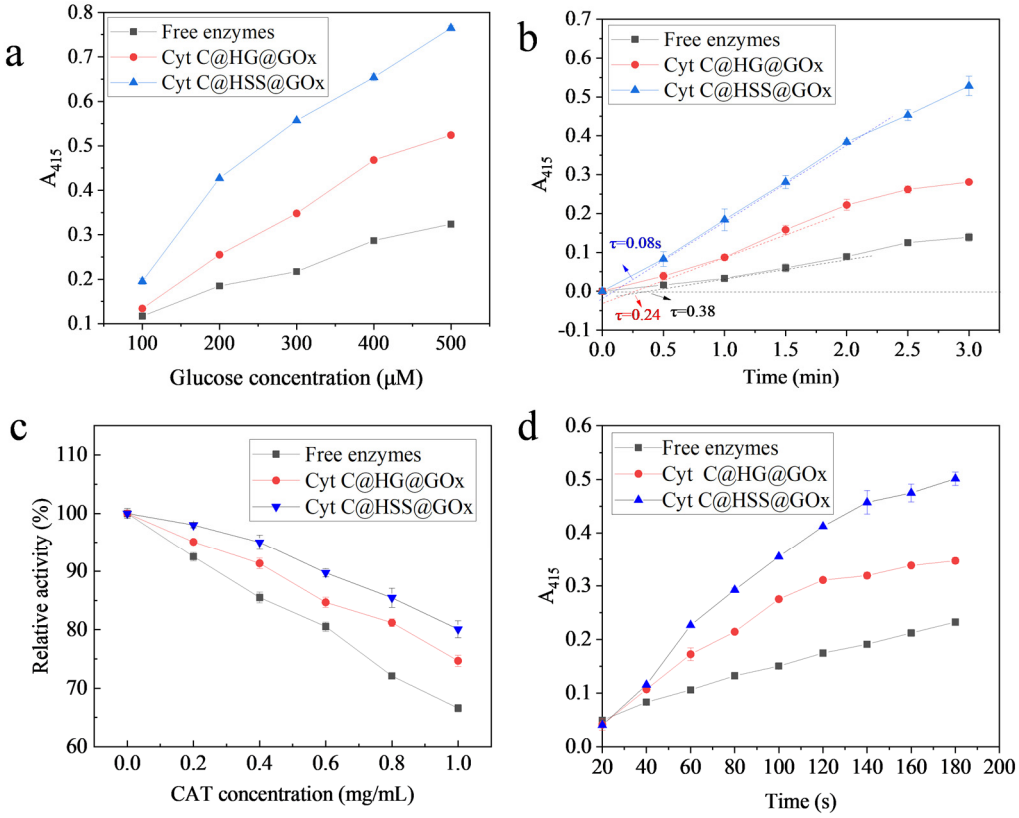

Fig. 6 Free enzymes, Cyt C@HG@GOx and Cyt C@HSS@GOx Changes in absorbance values for different substrate concentrations (a); reaction time (b); (c) Changes in absorbance values of Free enzymes, Cyt C@HG@GOx and Cyt C@HSS@GOx with reaction time after CAT addition; (d) Changes in absorbance values of free enzymes, Cyt C@HG@GOx and Cyt C@HSS@GOx at different CAT concentrations.

To further verify the substrate channeling effect, CAT was introduced as a competitor to Cyt C. The reaction was carried out in the existence of free CAT. Since the intermediate H_2O_2 competes with CAT in the second stage of the reaction, the presence of CAT leads to a reduction in the catalytic rate of the two-enzyme cascade; Consequently, varying concentrations of CAT were introduced into free Cyt C and GOx, as well as into the immobilized enzyme Cyt C@HSS@GOx, The enzyme activities of free cytosolic C and GOx as well as the immobilized enzyme Cyt C@HSS@GOx decreased progressively with increasing concentrations of added CAT. This was attributed to the ability of CAT to inhibit the production of the reaction products catalyzed by the second step of enzyme Cyt C. Furthermore, the increase in CAT concentration resulted in enhanced inhibition (Fig. 6c). Moreover, a slight reduction in the yield of end products was noted in the

compartmentalized co-immobilized system relative to the free system, across a range of reaction times and at a constant enzyme concentration (Fig. 6d). The Cyt C@HSS@GOx exhibited a smaller value of τ than the other two, indicating a greater substrate channeling effect and consequently a more rapid targeted transfer and conversion of the intermediate. The assignment effectively isolates the enzymes in their respective compartments, thereby allowing efficient substrate channeling and minimizing interference from competing reactions [39]. In conclusion, Cyt C@HSS@GOx exhibits a reduced mass transfer resistance to the substrate, this facilitates increased attachment between substrate and enzyme. The hollow structure allows the enzyme to reach a fixed but not rigid state, which is conducive to enhancing enzyme activity [40, 41].

3.4 Stability and reusability

The stability and reusability of Cyt C@HSS@GOx were evaluated. The immobilized enzyme demonstrated superior stability compared to the free enzyme under extreme pH and temperature. The experimental findings demonstrate that Cyt C@HSS@GOx maintains approximately 60% of its relative activity under acid-base conditions, while the free enzymes exhibited a retention of less than 50% (Fig. 7a)，following treatment at 60°C for 100 minutes, it was observed that Cyt C@HSS@GOx retained over 70% of its initial activity, but free enzymes decreased to less than 50% (Fig. 7b)， after 40 days of storage, Cyt C@HSS@GOx activity declined to about 60%, with free enzymes at just under 40% (Fig. 7d). Furthermore, after seven repetitions, Cyt C@HSS@GOx retained 71.25% of its initial activity (Fig. 7c), indicating excellent reusability. This is attributed to the fact that during in situ embedding, the enzyme is typically confined to the mesoporous lumen of the matrix, which limits the extent of structural alterations to the external environment [42].

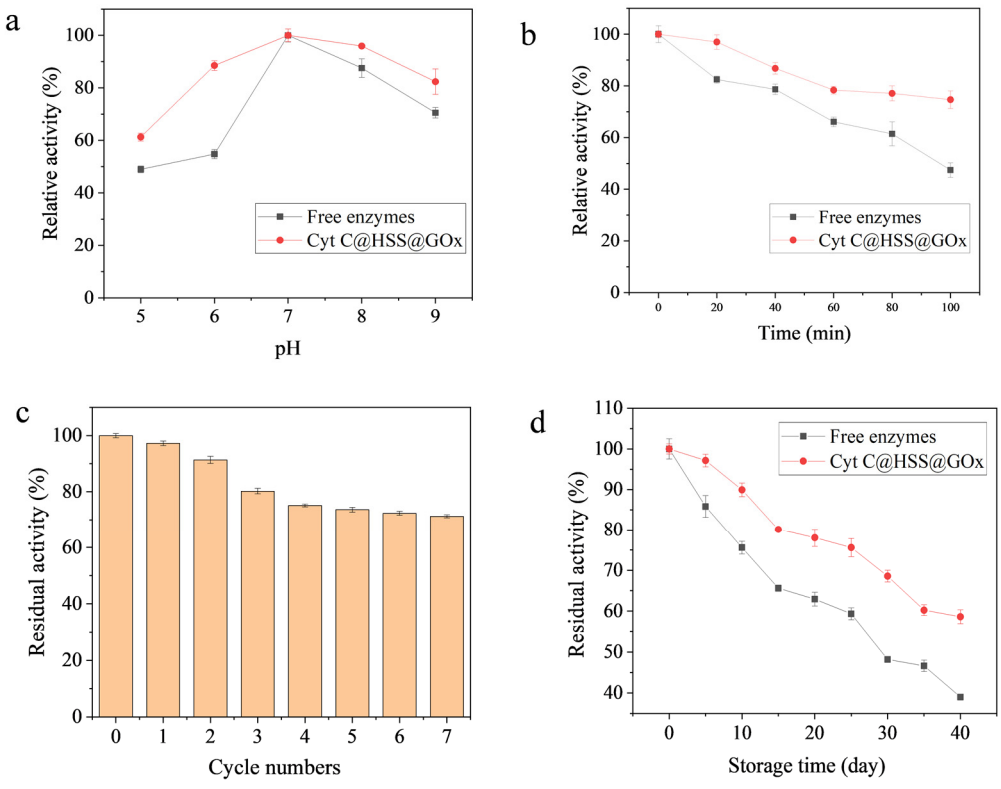

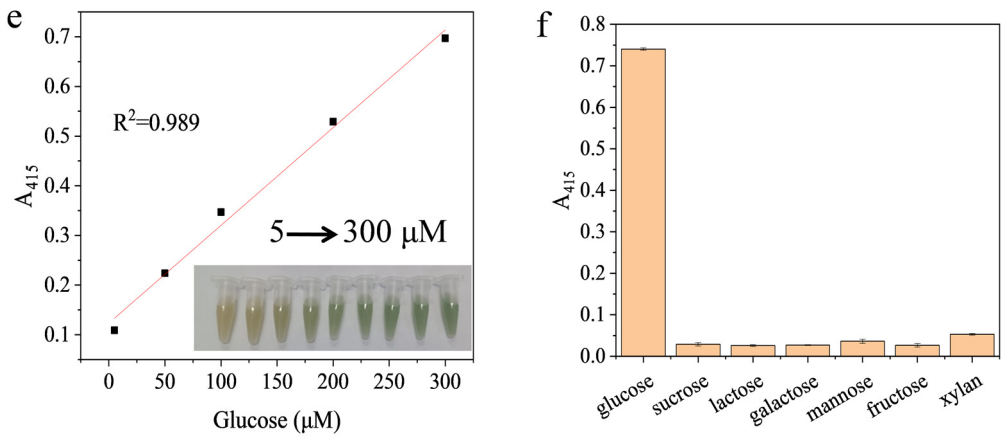

Fig. 7 Free enzymes and Cyt C@HSS@GOx (a) pH stability; (b) temperature stability at 80°C; (c) reusability of Cyt C@HSS@GOx; (d) Free enzymes and Cyt C@HSS@GOx storage stability; (e) detection of glucose concentrations of 5-300 μmol/L; (f) selectivity of Cyt C@HSS@GOx for 50 μmol/L glucose compared to 5 mmol/L sucrose, lactose, galactose, mannose, fructose and xylan.

3.5 Glucose detection

In order to demonstrate the validity of the multi-enzyme immobilization, the effectiveness of the Cyt C@HSS@GOx for glucose detection was determined by colorimetric method [43]. The results showed that Cyt C@HSS@GOx was able to detect glucose concentration and showed a linear relationship with glucose concentration in the range of 5 to 300 μmol/L (Fig. 7e). The detection limit of Cyt C@HSS@GOx was determined with a reaction time of approximately three minutes and a detection limit of 0.38 μmol/L. Table 3 lists a comparison of Cyt C@HSS@GOx with several previously reported biocatalysts for the detection of glucose. It was found that Cyt C@HSS@GOx exhibited superior glucose detection capability compared to previous reports. Additionally, The selectivity and immunity of Cyt C@HSS@GOx was assessed by measuring the absorbance values of Cyt C@HSS@GOx in the presence of different interferents including sucrose, lactose, galactose, mannose, fructose and xylan (A415). The concentration of glucose was found to be 50 μmol/L, while several other compounds were detected at a concentration of 5 mmol/L. Nevertheless, no notable signal was discerned, despite the presence of sucrose, lactose, galactose, mannose, fructose and xylan at concentrations up to 10-folds higher than that of glucose (Fig. 7f). The results demonstrate that Cyt C@HSS@GOx exhibits a specific response to glucose.

Table 3 Comparison of this work with previous reports for the detection of glucose

Catalyst	LOD (μmol/L)	Reaction time (min)	Ref
Cyt C@HZIF-8/GOx	0.8	10	[16]
mMOFs/GOxHRP	0.54	3	[44]
CHIT/CAR	5	60	[45]
ZnO/SiNWs	12	20	[46]
HAZNMs	50	20	[47]
CytC@HSS@GOx	0.38	3	This work

To verify the practicability of our biosensor, the Cyt C@HSS@GOx was applied in real samples for glucose detection. As shown in Table S2, the experiment utilized a glucose cube containing 4 g of glucose dissolved in 100 mL water (40 g/L), a 0.5% glucose oral solution (5 g/L), and Cola with a glucose concentration of 31.2 g/L by HPLC detection. A comparison was made between the actual glucose

concentration of the samples and the biosensor method, free enzymes, Cyt CGOx@HZIF-8 and Cyt C@HSS@GOx. It was found that the difference between the detected content and the actual glucose content was not significant, which indicated that this method could be used for glucose detection. However, the Cyt CGOx@HZIF-8 was unable to detect glucose, thereby confirming that the compartmentalized immobilized enzyme Cyt C@HSS@GOx exhibited superior sensitivity for glucose detection.

4. Conclusion

In summary, a spatially localized dual enzyme biosensor with layered shell-shell structure for glucose detection was developed. The dual enzyme exists in a free-like state in space, which enhances the channeling effect of the substrate. Moreover, the low-resistance mass transfer pathway facilitates directional transfer between enzymes, thereby enhancing catalytic activity. As a result, a substantial enhancement in catalytic efficiency, stability, and reusability has been observed in comparison to conventional randomly immobilized multi enzymes without no free-like state. Particularly, the spatially localized dual enzyme biosensor with layered shell-shell structure exhibited a low detection limit and high selectivity for glucose. Consequently, an efficient and stable multi-enzyme catalyst was designed by the strategy of immobilizing the multi-enzyme partition in a layered shell-shell structure for cascade catalysis, which is expected to have applications in biosensing and biocatalysis.

Acknowledgements

Dr. J. D. Cui thanks supports from the Science and Technology Program of Tianjin, China (project no. 20ZYJDJC00080), the Key Projects of Tianjin Natural Science Foundation, China (project no. 19JCZDJC38100), Project of Guangxi Key Research and Development program, China (project no. GuikeAB21238005), and Postgraduate Research Innovation project of Tianjin (project no. 2020YJSB122).

Conflict of interest

The authors declare that no conflict of interest exists

References

[1] T. Zhao, Y. Li, X. Zhang, H. Lyu, Z. Xie, A strategy for the accurate detection of glucose in human serum based on the IFE effect of up-transformed nanoparticles, Microchem. J. 186 (2023) 108363, http://doi.org/10.1016/j.microc.2022.108363

[2] S. Wild, G. Roglic, A. Green, R. Sicree, H. King, Global Prevalence of Diabetes: Estimates for the year 2000 and projections for 2030, Diabetes Care. 27 (5) (2004) 1047-1053, http://doi.org/10.2337/diacare.27.5.1047

[3] Y. Shu, T. Su, Q. Lu, Z. Shang, Q. Xu, X. Hu, Highly Stretchable Wearable Electrochemical Sensor Based on Ni-Co MOF Nanosheet-Decorated Ag/rGO/PU Fiber for Continuous Sweat Glucose Detection, Anal. Chem. 93 (48) (2021) 16222-16230, http://doi.org/10.1021/acs.analchem.1c04106

[4] P. Zhong, L. Zheng, Y. Yang, Y. Zhou, X. Liu, Q. Yang, J. Ren, Piezoelectric sensing of glucose oxidase activity of Aspergillus niger spores pretreated by different methods, Food Chem. 370 (2022) 130901, http://doi.org/10.1016/j.foodchem.2021.130901

[5] M. Tan, M. Ni, X. Liu, B. Qu, X. Lin, D. Jiang, Y. Yuan, H. Du, Surface adsorption guided design of semicrystalline nickel-iron hydroxide for highly-sensitive glucose sensing, Chem. Eng. J. 451 (2023) 138963, http://doi.org/10.1016/j.cej.2022.138963

[6] R. Zhang, S. Chatterjee, J. Ping, B. Liu, H.-S. Peng, Polymer organic framework-based ratiometric fluorescent probe for non-enzymatic glucose detection, Sensor Actuat B-Chem. 423 (2025) 136827, http://doi.org/10.1016/j.snb.2024.136827

[7] J. Liu, Y. Wang, M. He, X. Chen, C. Zhou, J. Li, Self-cascade catalytic system constructed using carbon dots and Au nanoparticles co-assembled on MIL-53(Fe)-NH2 as a three-in-one fluorescent nanozyme for multimodal detection of glucose and maltose in food, Food Chem. 468 (2025) 142485, http://doi.org/10.1016/j.foodchem.2024.142485

[8] H. An, J. Song, T. Wang, N. Xiao, Z. Zhang, P. Cheng, S. Ma, H. Huang, Y. Chen, Metal–Organic Framework Disintegrants: Enzyme Preparation Platforms with Boosted Activity, Angew. Chem., Int. Ed. 59 (38) (2020) 16764-16769, http://doi.org/10.1002/anie.202007827

[9] M. Bilal, S.A. Qamar, D. Carballares, Á. Berenguer-Murcia, R. Fernandez-Lafuente, Proteases immobilized on nanomaterials for biocatalytic, environmental and biomedical applications: Advantages and drawbacks, Biotechnol. Adv. 70 (2024) 108304, http://doi.org/10.1016/j.biotechadv.2023.108304

[10] O. Kreft, M. Prevot, H. Möhwald, G.B. Sukhorukov, Shell-in-shell microcapsules:: A novel tool for integrated, spatially confined enzymatic reactions, Angew. Chem. Int. Ed. 46 (29) (2007) 5605-5608, http://doi.org/10.1002/anie.200701173

[11] M. Marguet, C. Bonduelle, S. Lecommandoux, Multicompartmentalized polymeric systems: towards biomimetic cellular structure and function, Chem. Soc. Rev. 42 (2) (2013) 512-529, http://doi.org/10.1039/c2cs35312a

[12] K.S. Rabe, J. Müller, M. Skoupi, C.M. Niemeyer, Cascades in Compartments: En Route to Machine-Assisted Biotechnology, Angew. Chem., Int. Ed. 56 (44) (2017) 13574-13589, http://doi.org/10.1002/anie.201703806

[13] X. Zhang, L. Jing, F. Chang, S. Chen, H. Yang, Q. Yang, Positional immobilization of Pd nanoparticles and enzymes in hierarchical yolk–shell@shell nanoreactors for tandem catalysis, Chem. Commun. 53 (55) (2017) 7780-7783, http://doi.org/10.1039/C7CC03177G

[14] Z.N. Liu, B.D. Wang, S.H. Jin, Z.D. Wang, L. Wang, S. Liang, Bioinspired Dual-Enzyme Colloidosome Reactors for High-Performance Biphasic Catalysis, ACS Appl. Mater. Interfaces. 10 (48) (2018) 41504-41511, http://doi.org/10.1021/acsami.8b14321

[15] S. Arana-Peña, D. Carballares, R. Morellon-Sterlling, Á. Berenguer-Murcia, A.R. Alcántara, R.C. Rodrigues, R. Fernandez-Lafuente, Enzyme co-immobilization: Always the biocatalyst designers' choice…or not?, Biotechnol. Adv. 51 (2021) 107584, http://doi.org/10.1016/j.biotechadv.2020.107584

[16] Y. Feng, Y. Du, G. Kuang, L. Zhong, H. Hu, S. Jia, J. Cui, Hierarchical micro- and mesoporous ZIF-8 with core–shell superstructures using colloidal metal sulfates as soft templates for enzyme immobilization, J. Colloid Interface Sci. 610 (2022) 709-718, http://doi.org/10.1016/j.jcis.2021.11.123

[17] X.J. Shen, Y.J. Du, Z.X. Du, X.M. Tang, P.K. Li, J. Cheng, R.Y. Yan, J.D. Cui, Construction of enzyme@glutathione hybrid metal-organic frameworks: glutathione-boosted microenvironment fine-tuning of biomimetic immobilization for improving catalytic performance, Mater. Today Chem. 27 (2023) 101326, http://doi.org/10.1016/j.mtchem.2022.101326

[18] M. Dong, K.L. Liu, G.Q. Song, G.P. Ma, The MOF-on-MOF hybrids of MIL-101(Fe)@CoZn-ZIFs as efficient catalyst for the removal of deys from wastewater, J. Water Process Eng. 66 (2024) 105984, http://doi.org/10.1016/j.jwpe.2024.105984

[19] S.J. Lee, G.H.Y. Lee, M. Oh, MOF-on-MOF Growth: Inducing Naturally Nonpreferred MOFs and Atypical MOF Growth, Acc. Chem. Res. (2024) http://doi.org/10.1021/acs.accounts.4c00469

[20] H.D. Xu, J. Han, B. Zhao, R.G. Sun, G.Y. Zhong, G.R. Chen, Y. Yamauchi, B.Y. Guan, A facile dual-template-directed successive assembly approach to hollow multi-shell mesoporous metal-organic framework particles, Nat. Commun. 14 (1) (2023) 8062, http://doi.org/10.1038/s41467-023-43259-2

[21] S. Zaidi, M.I. Hassan, A. Islam, F. Ahmad, The role of key residues in structure, function, and stability of cytochrome-c, Cell. Mol. Life Sci. 71 (2) (2014) 229-255, http://doi.org/10.1007/s00018-013-1341-1

[22] M. Qiao, Y. Li, Y. Li, M. Chang, X. Zhang, S. Yuan, Unlocking of Hidden Mesopores for Enzyme Encapsulation by Dynamic Linkers in Stable Metal-Organic Frameworks, Angew. Chem., Int. Ed. 63 (51) (2024) e202409951, http://doi.org/https://doi.org/10.1002/anie.202409951

[23] Y.X. Feng, H.T. Hu, Z.C. Wang, Y.J. Du, L. Zhong, C.X. Zhang, Y.J. Jiang, S.R. Jia, J.D. Cui, Three-dimensional ordered magnetic macroporous metal-organic frameworks for enzyme immobilization, J. Colloid Interface Sci. 590 (2021) 436-445, http://doi.org/10.1016/j.jcis.2021.01.078

[24] L. Lin, S. Han, F. Meng, J. Li, K. Chen, E. Hu, J. Jiang, The influence of pore size and pore structure of silica-based material on the amine-modified adsorbent for CO2 capture, Sep. Purif. 340 (2024) 126735, http://doi.org/10.1016/j.seppur.2024.126735

[25] Q.Q. Zhu, W. Zhuang, Y. Chen, Z.K. Wang, B.V. Hernandez, J.L. Wu, P.P. Yang, D. Liu, C.J. Zhu, H.J. Ying, Z.H. Zhu, Nano-Biocatalysts of Cyt c@ZIF-8/GO Composites with High Recyclability via a de Novo Approach, ACS Appl. Mater. Interfaces. 10 (18) (2018) 16066-16076, http://doi.org/10.1021/acsami.8b00072

[26] L.H. Guo, R.W. He, G.S. Chen, H.S. Yang, X.X. Kou, W. Huang, R. Gao, S.Y. Huang, S.M. Huang, F. Zhu, G.F. Ouyang, A Synergetic Pore Compartmentalization and Hydrophobization Strategy for Synchronously Boosting the Stability and Activity of Enzyme, J. Am. Chem. Soc. 146 (25) (2024) 17189-17200, http://doi.org/10.1021/jacs.4c03286

[27] H. Xia, X. Zhong, Z. Li, Y. Jiang, Palladium-mediated hybrid biocatalysts with enhanced enzymatic catalytic performance via allosteric effects, Journal of Colloid and Interface Science. 533 (2019) 1-8, http://doi.org/10.1016/j.jcis.2018.08.052

[28] W. Shao, Y. Yao, G. Liu, W. Tang, Proton NMR studies of pyridine binding to cytochrome c, Inorg. Chem. 32 (26) (1993) 6112-6114, http://doi.org/10.1021/ic00078a033

[29] F. Han, N. Sari, Improvement of catalysis performance of pepsin and lipase enzymes by double enzyme immobilization method, RSC Advances. 14 (16) (2024) 11232-11243, http://doi.org/10.1039/d4ra00842a

[30] J.Y. Liang, S. Gao, J. Liu, M.Y.B. Zulkifli, J.T. Xu, J. Scott, V.C. Chen, J.F. Shi, A. Rawal, K. Liang, Hierarchically Porous Biocatalytic MOF Microreactor as a Versatile Platform towards Enhanced Multienzyme and Cofactor-Dependent Biocatalysis, Angew. Chem., Int. Ed. 60 (10) (2021) 5421-5428, http://doi.org/10.1002/anie.202014002

[31] W.T. He, Y.J. Gan, X.Y. Qi, H. Wang, H.Y. Song, P. Su, J.Y. Song, Y. Yang, Enhancing Enzyme Activity Using Hydrophilic Hollow Layered Double Hydroxides as Encapsulation Carriers, ACS Appl. Mater. Interfaces. 15 (29) (2023) 34513-34526, http://doi.org/10.1021/acsami.3c05237

[32] H.D. Neira, A.E. Herr, Kinetic Analysis of Enzymes Immobilized in Porous Film Arrays, Anal. Chem. 89 (19) (2017) 10311-10320, http://doi.org/10.1021/acs.analchem.7b02075

[33] H. Babaei, Z.G. Nejad, S. Yaghmaei, F. Farhadi, Co-immobilization of multi-enzyme cascade system into the metal-organic frameworks for the removal of Bisphenol A, Chem. Eng. J. 461 (2023) 142050, http://doi.org/10.1016/j.cej.2023.142050

[34] A.H. Elcock, G.A. Huber, J.A. McCammon, Electrostatic Channeling of Substrates between Enzyme Active Sites: Comparison of Simulation and Experiment, Biochem. 36 (51) (1997) 16049-16058, http://doi.org/10.1021/bi971709u

[35] H.O. Spivey, J. Ovádi, Substrate Channeling, Methods. 19 (2) (1999) 306-321, http://doi.org/https://doi.org/10.1006/meth.1999.0858

[36] Z. Wu, J. Shi, B. Zhang, Y. Jiao, X. Meng, Z. Chu, Y. Chen, Y. Cheng, Z. Jiang, Conjugated microporous polymers-scaffolded enzyme cascade systems with enhanced catalytic activity, Chin. J. Catal. 63 (2024) 213-223, http://doi.org/https://doi.org/10.1016/S1872-2067(24)60088-4

[37] W. Fan, K. Liang, J. Liang, One-pot spatial engineering of multi-enzymes in metal–organic frameworks for enhanced cascade activity, J. Mater. Chem. A. 12 (44) (2024) 30318-30328, http://doi.org/10.1039/D4TA06211F

[38] T. Man, C. Xu, X.-Y. Liu, D. Li, C.-K. Tsung, H. Pei, Y. Wan, L. Li, Hierarchically encapsulating enzymes with multi-shelled metal-organic frameworks for tandem biocatalytic reactions, Nat. Commun. 13 (1) (2022) 305, http://doi.org/10.1038/s41467-022-27983-9

[39] R.Z. Li, Z. Wu, X.C. Liu, H.X. Chen, X. Li, D.D. Fan, Z.S. Wu, Increasing Multienzyme Cascade Efficiency and Stability of MOF via Partitioning Immobilization, ACS Appl. Mater. Interfaces. 16 (26) (2024) 33235-33245, http://doi.org/10.1021/acsami.4c07487

[40] Y.J. Du, L.X. Zhao, Z.X. Geng, Z.B. Huo, H.H. Li, X.J. Shen, X.G. Peng, R.Y. Yan, J.D. Cui, S.R. Jia, Construction of catalase@hollow silica nanosphere: Catalase with immobilized but not rigid state for improving catalytic performances, Int. J. Biol. Macromol. 263 (2024) 130381, http://doi.org/10.1016/j.ijbiomac.2024.130381

[41] X.X. Meng, J.F. Shi, Z.H. Wu, W.P. Li, C. Yang, T. Qiu, Z.Y. Jiang, Bioactive Covalent Organic Framework Capsules for Lactate Synthesis, ACS Sustainable Chem. Eng. 11 (25) (2023) 9349-9358, http://doi.org/10.1021/acssuschemeng.3c00674

[42] Y.S. Jiao, Y. Nan, Z.H. Wu, X.Y. Wang, J.X. Zhang, B.Y. Zhang, S.Y. Huang, J.F. Shi, Mechanochemical synthesis of enzyme@covalent organic network nanobiohybrids, Appl. Mater. Today. 26 (2022) 101381, http://doi.org/10.1016/j.apmt.2022.101381

[43] L. Gu, S.L. Zeng, Z. Fan, W.Q. Qian, D.L. Qin, Z.X. Chen, L. Huang, S.Y. Bai, H.J. Xie, L. Gao, P. Wang, The application of a novel biomimetic enzyme p-BEs cascade catalytic platform for the rapid detection of glucose, Int. J. Biol. Macromol. 277 (2024) 134485, http://doi.org/10.1016/j.ijbiomac.2024.134485

[44] Y.X. Feng, Q.Q. Ma, Z.C. Wang, Q.L. Zhang, L.X. Zhao, J.D. Cui, Y.J. Du, S.R. Jia, Multivariate mesoporous MOFs with regulatable hydrophilic/hydrophobic surfaces as a versatile platform for enzyme immobilization, Chin. J. Catal. 60 (2024) 386-398, http://doi.org/10.1016/S1872-2067(24)60020-3

[45] I. Rassas, M. Braiek, A. Bonhomme, F. Bessueille, G. Rafin, H. Majdoub, N. Jaffrezic-Renault, Voltammetric glucose biosensor based on glucose oxidase encapsulation in a chitosan-kappa-carrageenan polyelectrolyte complex, Mater. Sci. Eng. 95 (2019) 152-159, http://doi.org/10.1016/j.msec.2018.10.078

[46] F.J. Miao, X.X. Lu, B.R. Tao, R. Li, P.K. Chu, Glucose oxidase immobilization platform based on ZnO nanowires supported by silicon nanowires for glucose biosensing, Microelectron. Eng. 149 (2016) 153-158, http://doi.org/10.1016/j.mee.2015.10.011

[47] R. Ahmad, N. Tripathy, M.Y. Khan, K.S. Bhat, M.S. Ahn, G. Khang, Y.B. Hahn, Hierarchically assembled ZnO nanosheets microspheres for enhanced glucose sensing performances, Ceram. Int. 42 (12) (2016) 13464-13469, http://doi.org/10.1016/j.ceramint.2016.05.134